

pubs.acs.org/JACS Article

Photoelectrochemical CO₂ Reduction to CO Enabled by a Molecular Catalyst Attached to High-Surface-Area Porous Silicon

Xiaofan Jia, ^L Eleanor Stewart-Jones, Jose L. Alvarez-Hernandez, Gabriella P. Bein, Jillian L. Dempsey, Carrie L. Donley, Nilay Hazari, Madison N. Houck, Min Li, James M. Mayer, Hannah S. Nedzbala, and Rebecca E. Powers



Cite This: J. Am. Chem. Soc. 2024, 146, 7998-8004



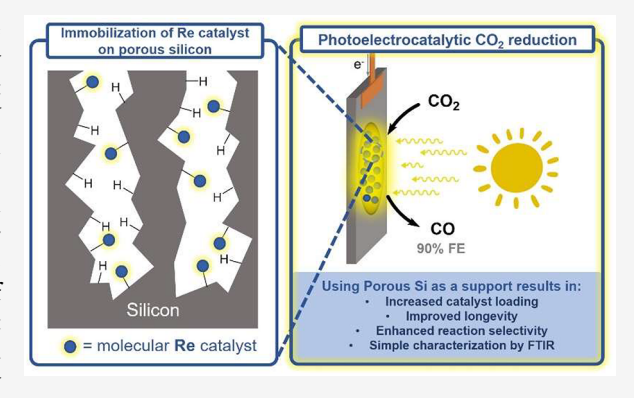
ACCESS

Metrics & More

Article Recommendations

s Supporting Information

ABSTRACT: A high-surface-area p-type porous Si photocathode containing a covalently immobilized molecular Re catalyst is highly selective for the photoelectrochemical conversion of CO_2 to CO . It gives Faradaic efficiencies of up to 90% for CO at potentials of $-1.7~\mathrm{V}$ (versus ferrocenium/ferrocene) under 1 sun illumination in an acetonitrile solution containing phenol. The photovoltage is approximately 300 mV based on comparisons with similar n-type porous Si cathodes in the dark. Using an estimate of the equilibrium potential for CO_2 reduction to CO under optimized reaction conditions, photoelectrolysis was performed at a small overpotential, and the onset of electrocatalysis in cyclic voltammograms occurred at a modest underpotential. The porous Si photoelectrode is more stable and selective for CO production than the photoelectrode generated by attaching the same Re catalyst to a planar Si wafer. Further, facile



characterization of the porous Si-based photoelectrodes using transmission mode FTIR spectroscopy leads to highly reproducible catalytic performance.

INTRODUCTION

The immobilization of molecular catalysts on solid supports can potentially combine the tunability of homogeneous catalysis with the practicality of heterogeneous catalysis. For photoelectrochemical processes such as CO₂ reduction, a semiconducting support can also serve as the light absorber, transferring electrons (or holes) to the molecular catalyst, but there is a need for supports that are easier to characterize, more durable, and give greater reproducibility in catalysis.² Si is an attractive semiconducting support because it is abundant, inexpensive, able to absorb light and separate charge, and its surface chemistry and electronic properties are well-studied.³ Nevertheless, reports of the immobilization of molecular catalysts on planar Si wafers are rare, and these systems often give poor and irreproducible catalytic performance⁴ due to their reactivity with oxygen, low surface area, modest catalyst surface coverages, and thus low activity.⁵

Porous Si, in contrast, is an easy to prepare and tunable material that can exhibit unusual stability against oxidation at room temperature⁶ and has surface areas that can be orders of magnitude greater than planar Si.⁷ Despite the widespread use of porous Si in biomedical sensing,⁸ drug delivery,⁹ and microelectronics,¹⁰ to our knowledge porous Si has yet to be used as a support for molecular catalysts.¹¹ Here, we describe the covalent attachment of a derivative of the well-known

molecular CO_2 reduction catalyst (bpy)Re(CO)₃Cl (bpy = 2,2'-bipyridine)¹² to *p*-type porous Si.¹³ The resulting hybrid photoelectrodes are more selective, stable, and reproducible photoelectrocatalysts for the reduction of CO_2 to CO compared to planar Si photoelectrodes. This suggests that porous Si-based materials may solve some of the challenges associated with finding inexpensive light-absorbing materials to immobilize molecular catalysts.

RESULTS AND DISCUSSION

Hydrogen-terminated porous *p*-type Si (H-porSi) was prepared using a previously described galvanostatic etching process with an aqueous HF solution in ethanol (see Figures 1a and S1).¹⁴ Transmission IR spectra of the H-porSi wafers exhibited SiH_x stretching bands at 2138 (SiH₃), 2116 (SiH₂), and 2089 (SiH) cm⁻¹, and a SiH₂ bending mode at 908 cm⁻¹ (Figures 1b and S2).¹⁵ Following a prior report,¹⁶ the intensity of these SiH_x bands was used to confirm the reproducibility of

Received: October 1, 2023 Revised: February 26, 2024 Accepted: February 27, 2024 Published: March 15, 2024





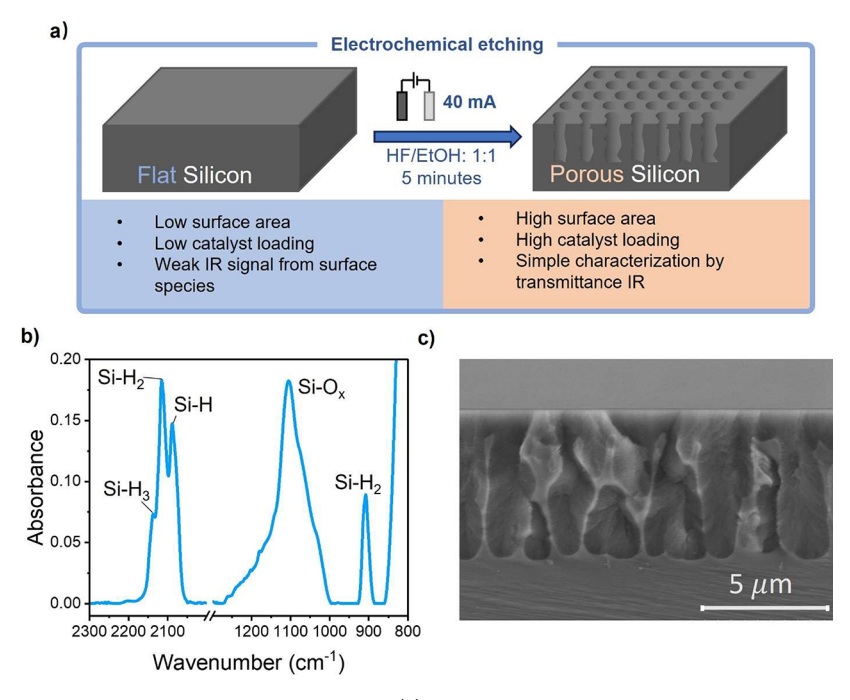


Figure 1. Preparation and characterization of freshly etched H-porSi. (a) Schematic showing the preparation of H-porSi. (b) FTIR spectrum, and (c) cross-sectional SEM image (9000× magnification).

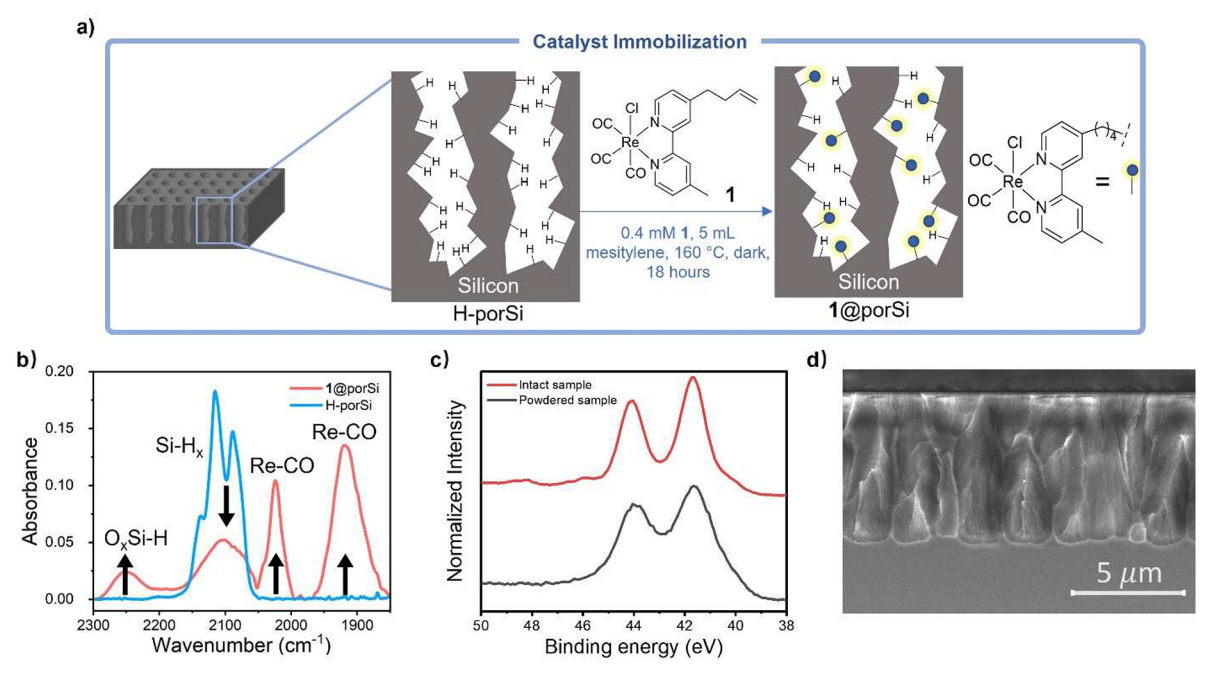


Figure 2. a) Schematic for the immobilization of 1 on porous p-type $(1-10 \ \Omega \ cm^{-1})$ Si to form 1@porSi. Characterization of 1@porSi, (b) FTIR and (c) Re 4f region XPS spectra. The XPS spectra are of an intact sample, which is representative of the top 10–15 nm of the surface, and a powdered sample, which was obtained by scratching of the porous material and mixing, and is representative of the entire pore. (d) Cross-sectional SEM image (8000× magnification).

the etching process between H-porSi wafers. The observed Si-O stretch at 1104 cm⁻¹ is intrinsic to the Czochralski (Cz)-type Si wafers, which contain interstitial oxygen atoms, ¹⁷ and the intensity of the Si-O stretch was similar before and after galvanostatic etching. X-ray photoelectron spectroscopy (XPS) of the H-porSi wafer showed a peak at 99.9 eV and a small, board feature at 100.7 eV (Figures S3 and S4), which is typical for hydrogen-terminated Si with a slightly oxidized surface. ¹⁸ Surface area measurements using a nitrogen isotherm

established a BET surface area of approximately 200 m²/g (Figure S5), similar to other examples of porous Si,¹⁹ and a surface roughness factor (measured vs geometric surface area) of 10^4 . Cross-sectional SEM images of the H-porSi wafers showed a pore depth of ~3.2 μ m (Figure 1c), with a sponge-like internal pore structure with roughened walls. Overall, H-porSi can be easily and reproducibly made and characterized and is stable upon exposure to O₂ under ambient conditions (Figures S6 and S7), which is crucial for achieving

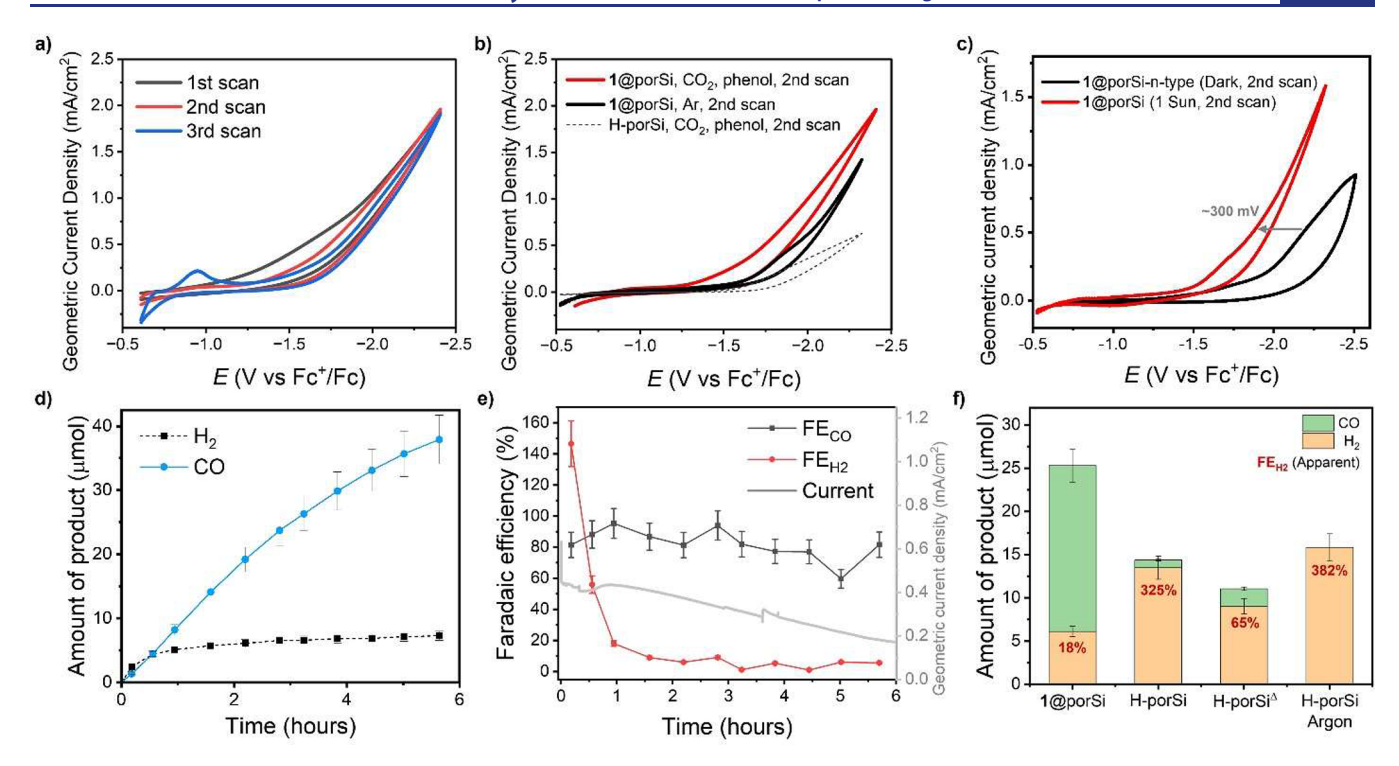


Figure 3. Photoelectrochemical performance using 1@porSi as the working electrode. (a) Three consecutive cyclic voltammogram scans of 1@ porSi under CO_2 with 100 mM phenol. (b) Second scan cyclic voltammograms of 1@porSi under CO_2 with 100 mM phenol (red), under Ar (black), and of H-porSi with 100 mM phenol under CO_2 (dashed). (c) Cyclic voltammograms of 1@porSi (red) and 1@porSi-n-type (black, recorded in the dark) with 100 mM phenol. (d) Cumulative amounts of CO and H_2 versus time and (e) FE at each individual time point and catalytic current versus time in a CPE experiment at -1.71 V versus Fc^+/Fc . (f) Comparison of product distributions, total charge passed, and apparent FE for H_2 from four 95 min CPE experiments with 1@porSi, a freshly etched H-porSi wafer, a H-porSi $^\Delta$ wafer heated (160 °C) in mesitylene for 18 h (without any Re catalyst) all under CO_2 , and a freshly etched H-porSi wafer under 1 atm Ar. Cyclic voltammograms and CPE were performed with 1 sun illumination (except for 1@porSi-n-type) in MeCN saturated with the appropriate gas containing 100 mM phenol and 0.1 M TBAPF $_6$ electrolyte.

reproducible catalytic results. In particular, the ability to use transmission mode FTIR spectroscopy to characterize H-porSi is a major advantage over flat Si wafers and other conductive supports, such as doped graphene and C_7N_4 .

A Re complex with a pendant alkene, (Rbpy)Re(CO)3Cl (1, Rbpy = 4-(but-3-en-1-yl)-4'-methyl-2,2'-bipyridine),4e was attached to H-porSi via hydrosilylation (1@porSi, Figure 2a). The hydrosilylation reaction converts surface Si-H bonds to Si-C bonds and is a common strategy to covalently attach molecules to hydrogen-terminated Si surfaces. 13 In this case, catalyst 1 was covalently attached to the surface via a butyl linker (Figures S8-S10). After hydrosilylation, 1@porSi was rinsed with different solvents and subjected to a vacuum to remove any physisorbed 1 and residual solvent. To quantify the amount of Re attached to the surface, a wafer of 1@porSi was digested in acid and analyzed by inductively coupled plasma mass spectrometry (ICP-MS). A sample of 1@porSi with a geometric area of 1.2 cm² contained roughly 41 nmol of Re (Table S1). This is \sim 100 times more Re than a monolayer of 1 on a flat Si wafer of the same geometric area, though the fractional surface coverage of Re in 1@porSi is lower in comparison to flat Si. 4e

The transmittance FTIR spectrum of 1@porSi exhibited prominent ν (CO) bands at 2019 and 1922 cm⁻¹ (Figures 2b and S10). The position of the ν (CO) stretches is typical for "(bpy)Re(CO)₃Cl complexes,²⁰ with the lower energy band broader and likely composed of two overlapping CO stretches. ν (CO) intensities were used to judge the reproducibility of

catalyst attachment across samples of 1@porSi (Figure S11). Attachment of 1 reduced the intensity of the surface Si-H stretching bands at ~2100 cm⁻¹ by approximately 60%. Even though the immobilization was conducted under dry, oxygenfree conditions, the Si-O stretches at 1104 cm⁻¹ increased significantly, and a new peak was observed at 2250 cm⁻¹, corresponding to partially oxidized OSi-H groups.²¹ The observed spectral changes are caused by both the hydrosilylation reaction and some surface oxidation.

XPS provided additional evidence for the presence of an attached Re in 1@porSi (Figures 2c and S12-S15). Considering that XPS typically analyzes the top 10-15 nm of a material, which accounts for less than 1% of the pore depth of Si as judged by SEM, we employed two sampling methods to probe the distribution of Re in 1@porSi. First, an intact sample was analyzed to measure the elemental distribution of the top 10-15 nm of the pores. Second, a powdered sample was obtained by scratching and scraping only the pores off the Si wafer. XPS analysis of this powder provided an average distribution of elements throughout the porous area. Both XPS measurements exhibited a Re 4f doublet (41.5 eV for the $4f_{7/2}$ peak), which confirms the presence of Re(I) species throughout the porous structure. 22,23 Cross-sectional SEM confirmed that the internal pore structure of 1@porSi was similar to that of H-porSi, showing that the hydrosilylation reaction did not change the structure of the wafer (Figure 2d). EDS (energy-dispersive X-ray spectroscopy) mapping further validated the presence of Re in 1@porSi but could not

establish the location of Re within the porous structure due to overlap between the Re and Si emission lines (Figures S16 and S17).

The photoelectrochemical properties of 1@porSi were explored under 1 sun illumination in acetonitrile (MeCN) with 100 mM phenol in a custom cell (Figures S18 and S19). The first scan in cyclic voltammograms of 1@porSi is similar under Ar vs CO₂ atmospheres (Figures 3a and S20). In both cases, significant current is observed with an onset potential of about -1.0 V. However, there is a noticeable drop in current in the second and subsequent scans of 1@porSi under Ar, which is much less pronounced under CO₂. We hypothesize that the current in the first scan is dominated by an irreversible electrochemical response from the surface of porous Si, likely from Si-H bonds or surface states.²⁴ This electrochemical response is independent of the atmosphere (CO₂ or Ar) or the presence of 1 on the surface (Figure S21).

In subsequent scans, the cyclic voltammograms increasingly reflect the different catalytic processes occurring under CO2 and Ar (CO₂ reduction vs hydrogen evolution reaction). Consistent with this proposal, the current and shapes of the second scans are different under CO₂ and Ar and in the presence and absence of 1 (Figure 3b). No redox features associated with 1 could be discerned for 1@porSi (under CO₂ or Ar) using cyclic voltammetry or linear sweep voltammetry (Figures S22 and S23). This is likely due to 1@porSi being far from an ideal electrode for cyclic voltammetry, with a range of microenvironments (due to both diffusion gradients down the pores and roughness of the pore walls), tortuous diffusion pathways for electrolyte and substrates, and complex behavior of the Si photoelectrode under these conditions. ²⁵ As discussed further in Section SVI. of the Supporting Information, we conclude that standard electrochemical analyses of such electrodes do not directly report on the redox properties of adsorbates.

Photoelectrocatalytic reduction of CO2 by 1@porSi in a CO₂-saturated MeCN solution containing 100 mM phenol was examined with controlled potential photoelectrolysis (CPE) at -1.71 V versus Fc⁺/Fc with 1 sun illumination. Analyzing the headspace using gas chromatography²⁶ showed CO as the only carbon product, along with H₂ (Figures S24 and S25). The CPE experiment passed ~8 C of charge over ca. 5.5 h. After 5.5 h, GC analysis showed 36 μ mol of CO and 7 μ mol of H₂ (Figure 3d), with time-averaged Faradaic efficiencies for CO (FE_{CO}) and H₂ (FE_{H₂}) of 91(9) and 18(2)%, respectively (Figure 3e). The FE_{CO} remained relatively constant at 70-95% over 5.5 h, but the current decayed from ca. 0.4 to 0.2 mA (Figure 3e). The maximum current density for CO production is ~ 0.4 mA/cm², and based on the amount of Re estimated from ICP-MS, the TOF is 160 h⁻¹. These results were reproducible over different CPE experiments, within ±7%. Photoelectrochemical reduction of ¹³CO₂ under the standard conditions produced ¹³CO (by GC-MS, Figures S26-S28). Thus, CO₂ is the source of the CO generated in the reaction.

A photovoltage for electrocatalysis of approximately 300 mV was obtained by comparing the catalytic onset potentials of 1@ porSi versus a photoelectrode containing 1 immobilized on a degenerately doped n-type porous Si wafer using cyclic voltammetry (Figure 3c; see Figures S29—S31 for experimental details). The \sim 300 mV photovoltage is consistent with the many reported photovoltages using p-Si photoelectrodes (0.2 to 0.6 V).

The overpotential for the photoelectrocatalytic reduction of CO₂ is an important metric but is difficult to estimate in multicomponent solutions such as those studied in this work. The standard potential for CO₂ reduction to CO and H₂O in MeCN has been predicted in the presence of buffers.²⁸ Further, Matsubara carefully examined how the standard potential for 3 CO₂ to CO and 2 HCO₃⁻ is affected by water.²⁹ However, estimation of the equilibrium potential for the system described here is complicated by the absence of significant CO, H2O, and phenoxide at the outset of photoelectrocatalysis and by the reactions of these products with each other and with CO₂. We estimate the equilibrium potential under our electrocatalytic conditions is -1.6 V versus Fc⁺/Fc, as described in Section SX. of the Supporting Information. This is also the value that Matsubara derived for 3 CO₂ to CO and 2 HCO₃⁻ at low water activities. ^{29b} An equilibrium potential of -1.6 V implies that the CPE experiments in this work were performed at a small overpotential. The onset of photoelectrocatalysis (see Figure 3a) from cyclic voltammetry (\sim -1.2 V) occurred at an underpotential, suggesting a small, formal amount of storage of the photon energy under these conditions.

In preliminary experiments to explore how our system might be optimized, we performed a CPE experiment where the intensity of light was systematically decreased from 1 to 0.01 sun and then the irradiation stopped. The amount of CO produced was dependent on the intensity of light, although not linearly (Figure S25). After the irradiation was stopped, resubjecting the sample to 1 sun illumination returned the CPE to the original current. Effects of light intensity (and stirring) were also observed in linear sweep voltammetry experiments (Figures S22 and S23). In addition to the light intensity and mass transport, the moderate activity of 1 likely also constrains the catalytic performance of 1@porSi (see Section SVI. of the Supporting Information).

Control experiments evaluated the photoelectrocatalytic activity of H-porSi without any attached 1 (Figures 3f, S32, and S33). These experiments used our standard CPE conditions with either a freshly etched H-porSi wafer or an H-porSi^{Δ} wafer that was heated at 160 °C for 18 h in neat mesitylene (the hydrosilylation conditions without 1). These two control wafers formed predominantly H₂ with a small amount of CO (CO₂ reduction by H-terminated Si materials has been reported³⁰). Thus, the immobilization of 1 is crucial for generating significant quantities of CO, and porous Si by itself is not efficient for CO₂ reduction. Similarly, leaching of 1 into solution is not responsible for CO₂ reduction (see Section SXII. of the Supporting Information).

The 1@porSi hybrid photoelectrocatalyst performs dramatically better than the same Re catalyst attached to a planar p-doped Si wafer under the same catalytic conditions. 1@porSi reduces CO_2 to CO with 90% FE, while 1 on a planar wafer has a FE_{CO} of 18%. Further, 1@porSi generates CO for at least 5.5 h (Figure 3e), while 1 on a planar wafer loses catalytic activity after 15 min. XPS and FTIR spectra of 1@porSi before and after CPE showed that ~75% of the Re was still present after electrolysis in the form of complexes of the type (Rbpy)Re(CO)₃X (X = solvent or atom from support; see Figures S34-S38). Reproducible catalytic results are obtained using 1@porSi, with very similar kinetics, FEs, and current densities achieved over three trials (see Figures S39 and S40), while 1 on planar wafers gave irregular results. The reproducibility is, in part, due to our ability to gauge the

quality of the initial H-porSi wafer and surface coverage of 1 using transmission FTIR spectroscopy. This degree of control is rare in the immobilization of molecular catalysts on solid

The high selectivity for CO with 1@porSi is even more remarkable after a closer examination of H2 production. While the average FE_{H_2} is 18% over 5.5 h, it was 145% over the first 10 min of CPE and rapidly dropped to less than 10% for the remainder (Figure 3e). Even higher FE_H, values, >300%, were observed in 95 min photo-CPE experiments using the H-porSi wafers described above, under CO₂ or Ar (Figure 3f). These high FEs indicate that a single electron can generate multiple equivalents of H₂ from H-porSi with and without 1 on the surface. CPE experiments using deuterated phenol and analysis of the H₂/HD/D₂ formed, which are presented in the Supporting Information (Figures S41 and S42), suggest that the Si-H bonds on 1@porSi and H-porSi participate in this pathway. Such a noncatalytic pathway consuming the original SiH groups to form H2 could explain the high FEH, values and why little H_2 is produced after the first ~45 min (Figure 3d). In this scenario, the catalytic selectivity for CO is higher than the values given above and should increase with CPE over longer times.

CONCLUSIONS

In conclusion, the first hybrid photoelectrocatalyst using porous Si was prepared by hydrosilylating a Re-based molecular catalyst to hydrogen-terminated p-type porous Si. 1@porSi is a selective, long-lived, and reproducible photocathode for the conversion of CO₂ to CO, performing better than the same molecular catalyst identically attached to planar Si. While some of this improvement is likely a result of higher catalyst loading per geometric area with the porous substrate, the improved selectivity for CO and the stability of the hybrid catalyst would appear to depend on the porous morphology. The origin of how the local microenvironment within the pores affects catalysis is being explored. Overall, this study highlights the advantages of attaching molecular catalysts to semiconducting, porous, and high-surface-area Si for photoelectrocatalytic applications.

ASSOCIATED CONTENT

Supporting Information

The Supporting Information is available free of charge at https://pubs.acs.org/doi/10.1021/jacs.3c10837.

Procedures for selected experiments, characterizing data, electrochemical data, and microscopy images (PDF)

AUTHOR INFORMATION

Corresponding Authors

yale.edu

Nilay Hazari — The Department of Chemistry, Yale University, New Haven, Connecticut 06520, United States; o orcid.org/ 0000-0001-8337-198X; Email: nilay.hazari@yale.edu James M. Mayer - The Department of Chemistry, Yale University, New Haven, Connecticut 06520, United States;

orcid.org/0000-0002-3943-5250; Email: james.mayer@

Authors

Xiaofan Jia - The Department of Chemistry, Yale University, New Haven, Connecticut 06520, United States; o orcid.org/ 0000-0003-0425-5089

Eleanor Stewart-Jones - The Department of Chemistry, Yale University, New Haven, Connecticut 06520, United States

Jose L. Alvarez-Hernandez – The Department of Chemistry, Yale University, New Haven, Connecticut 06520, United States; orcid.org/0000-0002-1761-9024

Gabriella P. Bein - Department of Chemistry, University of North Carolina at Chapel Hill, Chapel Hill, North Carolina 27599, United States; orcid.org/0000-0003-1970-553X

Jillian L. Dempsey - Department of Chemistry, University of North Carolina at Chapel Hill, Chapel Hill, North Carolina 27599, United States; orcid.org/0000-0002-9459-4166

Carrie L. Donley - Department of Chemistry, University of North Carolina at Chapel Hill, Chapel Hill, North Carolina 27599, United States; orcid.org/0000-0003-0906-306X

Madison N. Houck - The Department of Chemistry, Yale University, New Haven, Connecticut 06520, United States Min Li - West Campus Materials Characterization Core, Yale University, West Haven, Connecticut 06516, United States

Hannah S. Nedzbala – The Department of Chemistry, Yale University, New Haven, Connecticut 06520, United States

Rebecca E. Powers – Department of Chemistry, University of North Carolina at Chapel Hill, Chapel Hill, North Carolina 27599, United States

Complete contact information is available at: https://pubs.acs.org/10.1021/jacs.3c10837

Author Contributions

¹X.J. and E.S.-J. made equal contributions.

Notes

The authors declare no competing financial interest.

ACKNOWLEDGMENTS

This work was solely supported as part of the Center for Hybrid Approaches in Solar Energy to Liquid Fuels (CHASE), an Energy Innovation Hub funded by the U.S. Department of Energy, Office of Science, Office of Basic Energy Sciences, under Award Number DE-SC0021173. H.S.N. acknowledges support through a National Science Foundation Graduate Fellowship (2021315253). The IR instrument used in this study was purchased in 2018 with funds from the U.S. National Institutes of Health (R01GM50422), from the Air Force Office of Scientific Research under award number FA9550-18-1-0420 to the Multidisciplinary Research Program of the University Research Initiative (MURI), "Molecular-Scale Studies of Liquid-Solid Interfaces in Electrochemical Processes" and from the Center for Molecular Electrocatalysis (CME), an Energy Frontier Research Center funded by the U.S. Department of Energy, Office of Science, Office of Basic Energy Sciences. This work made use of: (i) instrumentation (XPS) at the Chapel Hill Analytical and Nanofabrication Laboratory, CHANL, a member of the North Carolina Research Triangle Nanotechnology Network, RTNN, which is supported by the National Science Foundation, Grant ECCS-2025064, as part of the National Nanotechnology Coordinated Infrastructure, NNCI; (ii) equipment in the Chemical and Biophysical Instrumentation Center at Yale University that was purchased with funds from Yale University. The authors acknowledge the use of facilities and instrumentation supported by NSF through the UC San Diego Materials Research Science and Engineering Center (UCSD MRSEC) DMR-2011924. We thank Professor Michael Sailor for valuable discussions relating to porous Si, Yuanzuo Gao and Shang Bo for their assistance in preparing samples for ICP—MS, and Professor Alexander Miller for assistance in estimating the reaction overpotential.

REFERENCES

- (1) (a) Copéret, C.; Chabanas, M.; Petroff Saint-Arroman, R.; Basset, J.-M. Homogeneous and Heterogeneous Catalysis: Bridging the Gap through Surface Organometallic Chemistry. *Angew. Chem., Int. Ed.* 2003, 42, 156–181. (b) Serna, P.; Gates, B. C. Molecular Metal Catalysts on Supports: Organometallic Chemistry Meets Surface Science. *Acc. Chem. Res.* 2014, 47, 2612–2620. (c) Copéret, C.; Comas-Vives, A.; Conley, M. P.; Estes, D. P.; Fedorov, A.; Mougel, V.; Nagae, H.; Núñez-Zarur, F.; Zhizhko, P. A. Surface Organometallic and Coordination Chemistry toward Single-Site Heterogeneous Catalysts: Strategies, Methods, Structures, and Activities. *Chem. Rev.* 2016, 116, 323–421. (d) Witzke, R. J.; Chapovetsky, A.; Conley, M. P.; Kaphan, D. M.; Delferro, M. Nontraditional Catalyst Supports in Surface Organometallic Chemistry. *ACS Catal.* 2020, 10, 11822–11840.
- (2) (a) Bullock, R. M.; Das, A. K.; Appel, A. M. Surface Immobilization of Molecular Electrocatalysts for Energy Conversion. Chem. Eur. J. 2017, 23, 7626-7641. (b) Corbin, N.; Zeng, J.; Williams, K.; Manthiram, K. Heterogeneous Molecular Catalysts for Electrocatalytic CO₂ Reduction. Nano Res. 2019, 12, 2093-2125. (c) Liu, H.-Y.; Cody, C. C.; Jayworth, J. A.; Crabtree, R. H.; Brudvig, G. W. Surface-Attached Molecular Catalysts on Visible-Light-Absorbing Semiconductors: Opportunities and Challenges for a Stable Hybrid Water-Splitting Photoanode. ACS Energy Lett. 2020, 5, 3195-3202. (d) Wu, Y.; Liang, Y.; Wang, H. Heterogeneous Molecular Catalysts of Metal Phthalocyanines for Electrochemical CO₂ Reduction Reactions. Acc. Chem. Res. 2021, 54, 3149-3159. (e) Morikawa, T.; Sato, S.; Sekizawa, K.; Suzuki, T. M.; Arai, T. Solar-Driven CO₂ Reduction Using a Semiconductor/Molecule Hybrid Photosystem: From Photocatalysts to a Monolithic Artificial Leaf. Acc. Chem. Res. 2022, 55, 933-943.
- (3) Siffert, P.; Krimmel, E. Silicon: Evolution and Future of a Technology; Springer Science: New York, 2013.
- (4) (a) Huang, K.; Duclairoir, F.; Pro, T.; Buckley, J.; Marchand, G.; Martinez, E.; Marchon, J.-C.; De Salvo, B.; Delapierre, G.; Vinet, F. Ferrocene and Porphyrin Monolayers on Si(100) Surfaces: Preparation and Effect of Linker Length on Electron Transfer. ChemPhysChem 2009, 10, 963-971. (b) Fabre, B. Ferrocene-Terminated Monolayers Covalently Bound to Hydrogen-Terminated Silicon Surfaces. Toward the Development of Charge Storage and Communication Devices. Acc. Chem. Res. 2010, 43, 1509-1518. (c) Kumar, B.; Smieja, J. M.; Kubiak, C. P. Photoreduction of CO₂ on p-type Silicon Using Re(bipy-Bu^t)(CO)₃Cl: Photovoltages Exceeding 600 mV for the Selective Reduction of CO₂ to CO. J. Phys. Chem. C 2010, 114, 14220-14223. (d) Moore, G. F.; Sharp, I. D. A Noble-Metal-Free Hydrogen Evolution Catalyst Grafted to Visible Light-Absorbing Semiconductors. J. Phys. Chem. Lett. 2013, 4, 568-572. (e) Jia, X.; Nedzbala, H. S.; Bottum, S. R.; Cahoon, J. F.; Concepcion, J. J.; Donley, C. L.; Gang, A.; Han, Q.; Hazari, N.; Kessinger, M. C.; Lockett, M. R.; Mayer, J. M.; Mercado, B. Q.; Meyer, G. J.; Pearce, A. J.; Rooney, C. L.; Sampaio, R. N.; Shang, B.; Wang, H. Synthesis and Surface Attachment of Molecular Re(I) Complexes Supported by Functionalized Bipyridyl Ligands. Inorg. Chem. 2023, 62, 2359-2375. (5) (a) Morita, M.; Ohmi, T.; Hasegawa, E.; Kawakami, M.; Ohwada, M. Growth of Native Oxide on a Silicon Surface. J. Appl. Phys. 1990, 68, 1272-1281. (b) Niwano, M.; Kageyama, J. i.; Kurita, K.; Kinashi, K.; Takahashi, I.; Miyamoto, N. Infrared Spectroscopy Study of Initial Stages of Oxidation of Hydrogen-Terminated Si Surfaces Stored in Air. J. Appl. Phys. 1994, 76, 2157-2163. (c) Johnson, S. I.; Blakemore, J. D.; Brunschwig, B. S.; Lewis, N.

- S.; Gray, H. B.; Goddard, W. A.; Persson, P. Design of Robust 2,2'-Bipyridine Ligand Linkers for the Stable Immobilization of Molecular Catalysts on Silicon(111) Surfaces. *Phys. Chem. Chem. Phys.* **2021**, 23, 9921–9929.
- (6) In the Supporting Information, we have provided details about the rate of oxidation of the porous Si that we used in this study.
- (7) (a) Herino, R.; Bomchil, G.; Barla, K.; Bertrand, C.; Ginoux, J. L. Porosity and Pore Size Distributions of Porous Silicon Layers. *J. Electrochem. Soc.* **1987**, 134, 1994–2000. (b) Northen, T. R.; Woo, H.-K.; Northen, M. T.; Nordström, A.; Uritboonthail, W.; Turner, K. L.; Siuzdak, G. High Surface Area of Porous Silicon Drives Desorption of Intact Molecules. *J. Am. Soc. Mass Spectrom.* **2007**, 18, 1945–1949.
- (8) Dhanekar, S.; Jain, S. Porous Silicon Biosensor: Current Status. *Biosens. Bioelectron.* **2013**, *41*, 54–64.
- (9) Anglin, E. J.; Cheng, L.; Freeman, W. R.; Sailor, M. J. Porous Silicon in Drug Delivery Devices and Materials. *Adv. Drug Delivery Rev.* **2008**, *60*, 1266–1277.
- (10) Sailor, M. J.; Link, J. R. "Smart Dust": Nanostructured Devices in a Grain of Sand. Chem. Commun. 2005, 36, 1375–1383.
- (11) For examples of metal nanoparticle catalysts on porous Si see: (a) Yang, Y.; Wang, M.; Zhang, P.; Wang, W.; Han, H.; Sun, L. Evident Enhancement of Photoelectrochemical Hydrogen Production by Electroless Deposition of M-B (M = Ni, Co) Catalysts on Silicon Nanowire Arrays. ACS Appl. Mater. Interfaces 2016, 8, 30143–30151. (b) Lee, S. A.; Park, I. J.; Yang, J. W.; Park, J.; Lee, T. H.; Kim, C.; Moon, J.; Kim, J. Y.; Jang, H. W. Electrodeposited Heterogeneous Nickel-Based Catalysts on Silicon for Efficient Sunlight-Assisted Water Splitting. Cell Rep. Phys. Sci. 2020, 1, 100219. (c) Jun, S. E.; Kim, Y.-H.; Kim, J.; Cheon, W. S.; Choi, S.; Yang, J.; Park, H.; Lee, H.; Park, S. H.; Kwon, K. C.; Moon, J.; Kim, S.-H.; Jang, H. W. Atomically Dispersed Iridium Catalysts on Silicon Photoanode for Efficient Photoelectrochemical Water Splitting. Nature Commun. 2023, 14, 609.
- (12) Hawecker, J.; Lehn, J.-M.; Ziessel, R. Electrocatalytic Reduction of Carbon Dioxide Mediated by Re(bipy)(CO)₃ Cl(bipy= 2,2'-bipyridine). *J. Chem. Soc., Chem. Commun.* **1984**, 328–330.
- (13) (a) Linford, M. R.; Chidsey, C. E. D. Alkyl Monolayers Covalently Bonded to Silicon Surfaces. *J. Am. Chem. Soc.* **1993**, *115*, 12631–12632. (b) Lee, S. H.; Kang, J. S.; Kim, D. A Mini Review: Recent Advances in Surface Modification of Porous Silicon. *Materials* **2018**, *11*, 2557.
- (14) Sailor, M. J. 'Preparation of Micro-, Meso-, and Macro-Porous Silicon Layers'. In *Porous Silicon in Practice*; Sailor, M. J., Ed.; Wiley: New York, 2011.
- (15) (a) Dillon, A. C.; Robinson, M. B.; George, S. M.; Gupta, P. Effects of Hydrogen Coverage on Silicon Surface Reactivity. *MRS Online Proc. Libr.* **1992**, 259, 99. (b) Kato, Y.; Ito, T.; Hiraki, A. Initial Oxidation Process of Anodized Porous Silicon with Hydrogen Atoms Chemisorbed on the Inner Surface. *Jpn. J. Appl. Phys.* **1988**, 27, L1406
- (16) Schmeltzer, J. M.; Porter, L. A.; Stewart, M. P.; Buriak, J. M. Hydride Abstraction Initiated Hydrosilylation of Terminal Alkenes and Alkynes on Porous Silicon. *Langmuir* **2002**, *18*, 2971–2974.
- (17) Sinno, T.; Dornberger, E.; von Ammon, W.; Brown, R. A.; Dupret, F. Defect Engineering of Czochralski Single-Crystal Silicon. *Mater. Sci. Eng. R Rep.* **2000**, 28, 149–198.
- (18) (a) Cerofolini, G. F.; Galati, C.; Renna, L. Si 2p XPS Spectrum of the Hydrogen-Terminated (100) Surface of Device-Quality Silicon. *Surf. Interface Anal.* **2003**, *35*, 968–973. (b) Aureau, D.; Bouttemy, M.; Vigneron, J.; Chazalviel, J.-N.; Ozanam, F.; Etcheberry, A. XPS Analysis of Porous Silicon. *ECS Trans.* **2013**, *50*, 107–114.
- (19) Buriak, J. M.; Stewart, M. P.; Geders, T. W.; Allen, M. J.; Choi, H. C.; Smith, J.; Raftery, D.; Canham, L. T. Lewis Acid Mediated Hydrosilylation on Porous Silicon Surfaces. *J. Am. Chem. Soc.* **1999**, *121*, 11491–11502.
- (20) Stor, G. J.; Hartl, F.; van Outersterp, J. W. M.; Stufkens, D. J. Spectroelectrochemical (IR, UV/Vis) Determination of the Reduction Pathways for a Series of $[Re(CO)_3(\alpha\text{-diimine})L']^{0/+}$ (L' =

- Halide, OTf, THF, MeCN, n-PrCN, PPh₃, P(OMe)₃) Complexes. Organometallics 1995, 14, 1115–1131.
- (21) Gupta, P.; Dillon, A. C.; Bracker, A. S.; George, S. M. FTIR studies of $\rm H_2O$ and $\rm D_2O$ Decomposition on Porous Silicon Surfaces. Surf. Sci. 1991, 245, 360–372.
- (22) A small amount of a Re containing complex was also detected on the planar areas of the electrode that were not exposed to HF and converted into porous Si. These sections of the wafer are therefore covered in a thermal oxide, but some attachment of an alkene to oxidized silicon is possible. See: Mischki, T. K.; Donkers, R. L.; Eves, B. J.; Lopinski, G. P.; Wayner, D. D. Reaction of Alkenes with Hydrogen-Terminated and Photooxidized Silicon Surfaces. A Comparison of Thermal and Photochemical Processes. *Langmuir* 2006, 22, 8359–8365.
- (23) XPS also showed the presence of trace amounts of Re(0) and ReO_3 , indicating a small amount of decomposition and oxidation of 1 on the surface. See the blips in the spectra at 46 and 48 eV and shoulder at 40 eV in the intact spectrum (red) in Figure 2c.
- (24) Bard, A. J.; Fan, F.-R. F.; Gioda, A. S.; Nagasubramanian, G.; White, H. S. On the Role of Surface States in Semiconductor Electrode Photoelectrochemical Cells. *Faraday Discuss. Chem. Soc.* **1980**, *70*, 19.
- (25) (a) Buttry, D. A.; Anson, F. C. Electron Hopping vs. Molecular Diffusion as Charge Transfer Mechanisms in Redox Polymer Films. J. Electroanal. Chem. Interface Electrochem. 1981, 130, 333-338. (b) Punckt, C.; Pope, M. A.; Aksay, I. A. On the Electrochemical Response of Porous Functionalized Graphene Electrodes. J. Phys. Chem. C 2013, 117, 16076-16086. (c) Waelder, J.; Vasquez, R.; Liu, Y.; Maldonado, S. A Description of the Faradaic Current in Cyclic Voltammetry of Adsorbed Redox Species on Semiconductor Electrodes. J. Am. Chem. Soc. 2022, 144, 6410-6419. (d) Costentin, C. Cyclic Voltammetry to Study Dynamics of Ion Insertion in Porous Materials. Adv. Energy Sustainability Res. 2023, 2300242. (e) Keller, N. D.; Vecchi, P.; Grills, D. C.; Polyansky, D. E.; Bein, G. P.; Dempsey, J. L.; Cahoon, J. F.; Parsons, G. N.; Sampaio, R. N.; Meyer, G. J. Multi-Electron Transfer at H-Terminated p-Si Electrolyte Interfaces: Large Photovoltages under Inversion Conditions. J. Am. Chem. Soc. 2023, 145, 11282-11292.
- (26) The reaction solution was analyzed using ¹H NMR spectroscopy and no liquid products from CO₂ reduction were detected.
- (27) Laurans, M.; Wells, J. A. L.; Ott, S. Immobilising Molecular Ru Complexes on a Protective Ultrathin Oxide Layer of p-Si Electrodes Towards Photoelectrochemical CO₂ Reduction. *Dalton Trans.* **2021**, 50, 10482–10492.
- (28) (a) Pegis, M. L.; Roberts, J. A. S.; Wasylenko, D. J.; Mader, E. A.; Appel, A. M.; Mayer, J. M. Standard Reduction Potentials for Oxygen and Carbon Dioxide Couples in Acetonitrile and N,N-Dimethylformamide. *Inorg. Chem.* 2015, 54, 11883–11888. (b) Pegis, M. L.; Roberts, J. A. S.; Wasylenko, D. J.; Mader, E. A.; Appel, A. M.; Mayer, J. M. Correction to Standard Reduction Potentials for Oxygen and Carbon Dioxide Couples in Acetonitrile and N,N-Dimethylformamide. *Inorg. Chem.* 2020, 59, 8638.
- (29) (a) Matsubara, Y.; Grills, D. C.; Kuwahara, Y. Thermodynamic Aspects of Electrocatalytic CO₂ Reduction in Acetonitrile and with an Ionic Liquid as Solvent or Electrolyte. *ACS Catal.* **2015**, *5*, 6440–6452. (b) Matsubara, Y. Standard Electrode Potentials for the Reduction of CO₂ to CO in Acetonitrile—Water Mixtures Determined Using a Generalized Method for Proton-Coupled Electron-Transfer Reactions. *ACS Energy Lett.* **2017**, *2*, 1886–1891.
- (30) (a) Sun, W.; Qian, C.; He, L.; Ghuman, K. K.; Wong, A. P. Y.; Jia, J.; Ali, F. M.; O'Brien, P. G.; Reyes, L. M.; Wood, T. E.; Helmy, A. S.; Mims, C. A.; Singh, C. V.; Ozin, G. A. Heterogeneous Reduction of Carbon Dioxide by Hydride-Terminated Silicon Nanocrystals. *Nature Commun.* 2016, 7, 12553. (b) Dasog, M.; Kraus, S.; Sinelnikov, R.; Veinot, J. G. C.; Rieger, B. CO₂ to Methanol Conversion Using Hydride Terminated Porous Silicon Nanoparticles. *Chem. Commun.* 2017, 53, 3114–3117. (c) Qian, C.; Sun, W.; Hung, D. L. H.; Qiu, C.; Makaremi, M.; Hari Kumar, S. G.; Wan, L.; Ghoussoub, M.; Wood, T. E.; Xia, M.; Tountas, A. A.; Li, Y. F.; Wang,

L.; Dong, Y.; Gourevich, I.; Singh, C. V.; Ozin, G. A. Catalytic CO₂ Reduction by Palladium-Decorated Silicon–Hydride Nanosheets. *Nature Catal.* **2018**, *2*, 46–54.